Micellar Mimicry of Intermetallic C14 and C15 Laves Phases by Aqueous Lyotropic Self-Assembly

Carlos M. Baez-Cotto[†] *and Mahesh K. Mahanthappa*[†,‡,*]

[†]Department of Chemistry, University of Minnesota, 207 Pleasant St. SE, Minneapolis, MN 55455

[‡] Department of Chemical Engineering & Materials Science, University of Minnesota, 421 Washington Ave. SE, Minneapolis, MN 55455

* Email: maheshkm@umn.edu; +1 (612) 625-4599

ORCID

Mahesh K. Mahanthappa: 0000-0002-9871-804X

KEYWORDS liquid crystals • self-assembly • surfactants • Frank–Kasper phases • lyotropic phase • superlattices

Abstract

Concentration-dependent supramolecular self-assembly of amphiphilic molecules in water furnishes a variety of nanostructured lyotropic liquid crystals (LLCs), which typically display high symmetry bicontinuous network and discontinuous micellar morphologies. Aqueous dispersions of soft spherical micelles derived from small molecule amphiphile hydration typically pack into exemplary body-centered cubic and closest–packed LLCs. However, investigations of hydrated mixtures of the ionic surfactant tetramethylammonium decanoate loaded with 40 wt% *n*-decane (**TMADec-40**) revealed the formation of a high symmetry bicontinuous double diamond LLC, as well as cubic C15 and hexagonal C14 Laves LLC phases that mirror the $MgCu_2$ and $MgZn_2$ intermetallic structure types, respectively. Detailed small-angle X-ray scattering analyses demonstrate that the complex C15 and C14 LLCs exhibit large unit cells, in which twelve or more ~3–4 nm diameter micelles of multiple discrete sizes arrange into tetrahedral close packing arrangements with exceptional long-range translational order. The symmetry breaking that drives self-assembly into these low symmetry LLC phases is rationalized in terms of a frustrated balance between maximizing counterion-mediated micellar cohesion within the ensemble of oil-swollen particles, while simultaneously optimizing local spherical particle symmetry to minimize molecular-level variations in surfactant solvation.

The properties and ultimate applications of self-assembled soft materials stem from their mesoscale structures, which reflect local molecular packing arrangements that are controlled by a delicate balance of non-covalent interactions. A series of similar structural motifs arise from the self-assembly of block polymers,[1, 2] thermotropic liquid crystals (LCs),[3, 4] giant shape amphiphiles,[5, 6] and lyotropic liquid crystals (LLCs),[7, 8] including the formation of 1D layered structures (lamellae), 2D columnar phases, high symmetry bicontinuous 3D networks, and various 3D sphere packings. Depending on the size and symmetry of the molecular building blocks and the length scales at which they cooperatively self-assemble, these supramolecular structures exhibit useful physical properties as photonic band gap materials and Bragg reflectors,[9-11] templates for catalytically useful microporous and mesoporous metal oxides,[12, 13] and encapsulation media and targeted delivery vehicles for molecular therapeutics.[14-16] Broadening the existing and future potential applications of these designer soft materials motivates studies of the fundamental principles underlying their "bottom up" self-assembly into ever more complex structures with unique and exciting properties.

A cursory survey of the Periodic Table reveals that numerous metallic elements form high symmetry structures containing 2–4 particles per unit cell, exemplified by body-centered cubic (BCC), face-centered cubic (FCC), and hexagonally closest-packed (HCP) structures.[17] While the latter two arrangements may be intuitively rationalized as hard sphere packings that regularly fill space at maximum density, detailed electronic structure models account for all three atomic packings in terms of pairwise interparticle interactions mediated by a "sea of free electrons."[18] However, certain metallic elements (*e.g.*, Mn, Ta,[19] and Pu[20]) and numerous metal alloys form low–symmetry crystals with gigantic unit cells comprising ≥ 7 particles, known as Frank–Kasper (FK) phases.[17] In their seminal papers nearly 60 years ago, Frank and Kasper recognized that the

fundamental atomic packing motifs in these low symmetry crystals are tetrahedral arrangements of atoms with an average of > 12 neighboring lattice sites.[21, 22] Thus, each atomic position in a FK phase sits within a cluster with a coordination number CN = 12, 14, 15, or 16. Numerous FK metal alloy phases have been experimentally documented, and they are now well-recognized as 3D periodic approximants of quasicrystals. Quasicrystals, which exhibit local rotational symmetry with no long-range translational order, may thus be viewed as FK phases with infinitely large unit cells.[23, 24] The formation of these complex FK phases is thought to arise from the simultaneous optimization of both metallic bonding and Fermi surface sphericity, the latter of which describes the distribution of free electron velocities within a metallic solid.[25]

While soft spherical particles arising from molecular self-assembly are often reported to form FCC, HCP, and BCC lattices, a series of recent examples illustrate their propensity to form FK phases that are structurally analogous to those of metals and their alloys.[26-28] The first aqueous lyotropic cubic A15[29] and C15 Laves[30, 31] mesophases of minimally hydrated small molecule surfactants were first reported over 25 years ago, although the physical principles governing their formation remained obscure until only recently.[32, 33] A number of reports over the last 15 years have described FK A15 and σ phases, as well as related dodecagonal quasicrystals, in thermotropic LCs of wedge-type dendrons,[34-36] linear diblock and multiblock polymers,[37-39] and giant shape amphiphiles.[5, 6] Furthermore, specific thermal processing protocols can even coax compositionally asymmetric diblock polymers to self-assemble into tetrahedrally closest-packed cubic C15 and hexagonal C14 Laves phases.[40, 41] A distinguishing feature of these complex soft matter phases is the spontaneous formation of two or more symmetry-equivalent classes of particles with discrete sizes. FK micellar packings in pseudo-single component block polymers apparently arise from local minimization of unfavorable core–corona interactions for each

particle, and simultaneous global optimization of cohesive van der Waals contacts across the ensemble of particles (*i.e.*, packing at uniform density to minimize 3D packing frustration).[32,42]

However, the formation of aqueous LLC FK phases of normal surfactant micelles embedded in a water matrix is governed by different phenomena, due to the lack of interparticle van der Waals contacts. Kim *et al.* recently reported that normal micelles of a dianionic alkylphosphonate surfactant form lyotropic A15 and BCC phases, along with a more complex LLC FK σ mesophase.[33] On the basis of molecular dynamics (MD) simulations, they rationalized the formation of these phases in terms of maximization of electrostatic interparticle cohesion, while minimizing molecular-level variations in surfactant solvation. However, the generality of these phenomena, the possibility of accessing other complex micellar FK LLCs, and the origins of complex phase selection in sphere-forming LLC materials remain in question.

In this report, we describe the unexpected aqueous LLC phase behavior of a mixture of a simple ionic surfactant loaded with a hydrocarbon oil that forms a variety of structured microemulsions. Specifically, we use small-angle X-ray scattering to investigate the water concentration–dependent self-assembly characteristics of hydrated tetramethylammonium decanoate loaded with 40 wt% *n*-decane. These studies expose the remarkable ability of these simple ternary compositions to form a normal bicontinuous double diamond, and three very different spherical micelle morphologies: a BCC packing, a cubic C15 Laves phase, and an unexpected LLC C14 Laves phase. Retrostructural analyses based on high-resolution synchrotron X-ray data, in conjunction with geometric considerations of micelle sphericity, provide insights into the cohesive forces that stabilize the complex C15 and C14 Laves structures.

Results and Discussion

In the course of our studies of the aqueous microemulsion phase behaviors of mixtures of single-tail alkylcarboxylate surfactants with low molecular weight hydrocarbon oils, we observed the formation of a set of structured LLC mesophases with unusual physical properties (*vide infra*). Herein, we focus exclusively on a series of LLC samples derived from a mixture of tetramethylammonium decanoate (**TMA-Dec**) with 40 wt% *n*-decane that was variably hydrated with ultrapure water. Analytically pure samples of **TMA-Dec** were produced by deprotonating commercially available decanoic acid with $(CH_3)_4NOH$ in CH_3OH. Microemulsion samples were then prepared stepwise by: (1) combining carefully measured amounts of **TMA-Dec** with 40 wt% *n*-decane by three cycles of high-speed centrifugation and hand-mixing to produce a composition designated **TMADec-40**, after which (2) ultrapure water was added and thoroughly mixed by another three cycles of iterative high-speed centrifugation and hand-mixing (see Methods Section for synthetic details and sample preparation protocols).

Using synchrotron small-angle X-ray scattering (SAXS), we systematically explored the temperature-dependent LLC phase behavior of **TMADec-40** in the range of surfactant headgroup hydration numbers w_0 = (total moles H_2O)/(mol **TMA-Dec**) = 2–30 between T = 23–100 °C. The reported w_0 explicitly accounts for the total amount of water present in the sample arising from addition of water to the analytically pure surfactant hydrate (see Methods Section). Optically non-birefringent LLCs having w_0 = 26–30 exhibit six SAXS peaks located at scattering wavevector ratios $q/q^* = \sqrt{2}, \sqrt{4}, \sqrt{6}, \sqrt{10}, \sqrt{12}$, and $\sqrt{14}$ ($q^* = 0.1688$ Å^{-1}), consistent with a BCC arrangement of spherical micelles with a unit cell parameter $a \approx 5.3$ nm (Figure 1). Upon raising the temperature of these samples, we find that the sharp Bragg scattering peaks of the BCC lattice melt into the broad scattering of a disordered, fluid micellar solution. SAXS analyses

revealed that this lattice order-disorder transition is fully reversible (see Supporting Information Figure S1). We note that addition of excess water to these LLCs results in the formation of fluid solutions of micelles that are visually homogeneous, implying that this BCC phase is a normal micellar LLC comprising oil-swollen particles in an aqueous matrix.

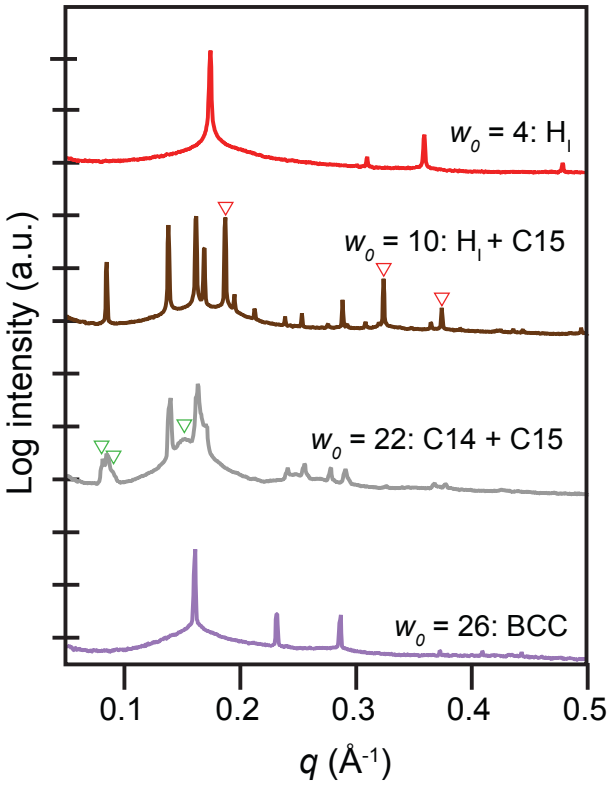

Figure 1. Azimuthally-integrated one-dimensional intensity $I(q)$ *versus* scattering wavevector q profiles for aqueous LLCs of **TMADec–40** at surfactant headgroup hydration numbers w_0 = 4, 10, 22, and 26, which respectively correspond to a hexagonally–packed cylinders phase (H_I), H_I/C15 coexistence (red markers indicate the (10), (11), and (20) peaks of the H_I structure), coexisting C14 and C15 Laves phases (green markers indicate the positions of the (100), (101), and (103) peaks of the C14 structure), and a body-centered cubic (BCC) spheres morphology.

Upon decreasing the **TMADec-40** hydration number to w_0 = 24, we obtained an extremely tacky, high modulus, optically non-birefringent LLC that was qualitatively stiffer than the above BCC phases. SAXS analyses reveal that this sample presents an unexpected scattering signature with > 30 sharp Bragg scattering peaks and an unusual intensity pattern (Figure 2A and Figure S2). These peaks markedly sharpen after thermal annealing by heating to 100 °C and cooling to ambient temperature. The combination of lower intensity low q peaks and the higher intensity peaks at intermediate q = 0.14–0.19 Å^{-1} is reminiscent of the SAXS patterns of low symmetry FK A15 and σ phases,[39, 6, 33] possibly suggesting another complex lyotropic sphere packing. Detailed analysis of this scattering pattern revealed that the underlying structure is consistent with the hexagonal $P6_3/mmc$ symmetry with unit cell parameters a = 8.53 nm and c = 13.89 nm with c/a = 1.628 (Figure 2A and Table S1). While this scattering signature also conforms to the lower space group symmetries $P6(-)c2$, $P6_3mc$, $P6_322$, $P3(-)1c$, we prefer the highest symmetry $P6_3/mmc$ space group according to established crystallographic convention. Although this structural symmetry is the same as that of HCP spheres with a nearly ideal $c/a = \sqrt{8}/3 \approx 1.633$,[17] the large unit cell parameters for this packing of ~3 nm diameter micelles and the unique peak intensity pattern imply a more complex structure. Furthermore, the SAXS peak intensity pattern differs substantially from that of previously reported HCP LLC sphere packings (see Figure S2).[43-45] Also, the highest Miller indices of the observed SAXS peaks suggest exceptional long-range translational ordering at length scales > 100 nm. This scattering signature remains well-defined and sharp up to T = 80 °C, above which the sharp peaks for this new phase are superposed on a broad scattering peak corresponding to disordered micelles; this two–phase coexistence is precedented and expected in ternary LLCs on the basis of Gibbs Phase Rule.[46, 47] The striking resemblance of this diffraction pattern with those simulated and experimentally observed for the

hexagonal C14 Laves phases reported by Hajiw *et al*. in Au nanoparticle superlattices[48] and by Bates and co-workers in diblock polymers[40, 41] strongly suggests that this sample comprises an aqueous lyotropic C14 mesophase.

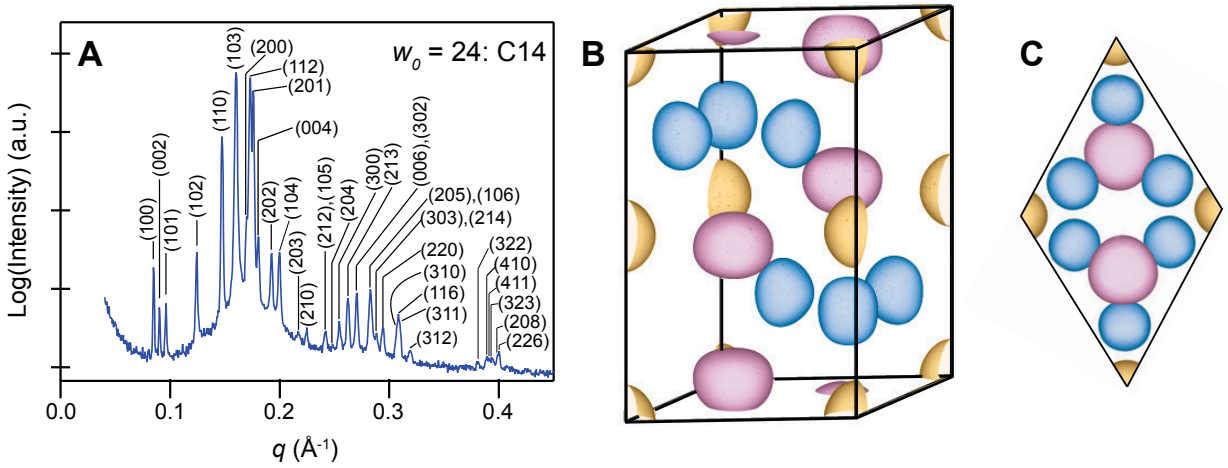

Figure 2. (A) SAXS powder diffraction profile obtained at T = 25 °C for the aqueous C14 Laves phase LLC derived from **TMADec–40** at w_0 = 24 with unit cell parameters a = 8.53 nm and c = 13.89 nm (c/a = 1.628), which exhibits at least 30 distinct, instrument resolution-limited peaks. (B) Perspective view of the electron density map for this C14 Laves phase (90% isosurface) derived from the experimental SAXS data, indicating the formation of three classes of symmetry-equivalent micelles located in the *2a* (*gold*), *4f* (*pink*), and *6h* (*blue*) Wyckoff positions. (C) View of the electron density map for the C14 unit cell along the *c*-axis.

We used a combination of Le Bail refinement[49] of the SAXS data acquired at 25 °C to extract the structure factor intensities for each scattering peak and established charge-flipping algorithms[50] to reconstruct an electron density map for this C14 Laves LLC (Figures 2B and 2C). The resulting electron density map predicts the experimentally observed SAXS pattern with high fidelity (residual factor R = 1; see Supporting Information for methodological details). The C14 unit cell contains 12 quasispherical micelles of three discrete volumes in an arrangement analogous to the $MgZn_2$ intermetallic structure.[17] From the 90% electron density isosurface depicted in Figure 2, we estimate the micelle radii to be ~1.55, 1.72, and 1.53 nm for the *2a*, *4f*, and *6h* micelles, respectively (these values are approximate due the aspherical nature of the

particles). The large variations in micelle radii and volumes necessarily imply that each class of symmetry-equivalent micelles must contain different numbers of oil and surfactant molecules, instead of each micelle having the same average structure and chemical composition. Based the mass densities of the chemical constituents of this C14 LLC phase, we estimate that *n*-decane constitutes ~35 vol% of each micelle core and that the number of surfactants per micelle is $N \approx$ 51, 63, and 49 for the respective *2a*, *4f*, and *6h* lattice sites (see Supporting Information for the detailed calculations). Excluding the hydrated counterions, the micelles may be viewed as core-shell particles with an oily core sheathed by a surfactant shell that is ~0.45–0.50 nm thick. Finally, the soft facets of each micelle face those of their nearest neighbors and thus mimic the underlying Wigner-Seitz (W–S) cells of the C14 lattice. However, we note that these oil-laden particles occupy only ~22–26 vol% of their respective W–S cells, which are otherwise filled with hydrated $(CH_3)_4N^+$ counterions. The micellar faceting and discrete micelle size distribution mirror those previously observed by Kim *et al*. in LLC FK A15 and σ phases.[33] We return to the origins of these unusual features of the electron density map in the discussion below.

Azimuthally-integrated SAXS intensity profiles for **TMADec-40** LLCs in the hydration range w_0 = 12-20 typically exhibit at least 20 scattering maxima located at $q/q^* = \sqrt{3}, \sqrt{8}, \sqrt{11}, \sqrt{12}, \ldots$ ($q^* = 0.0493$ Å^{-1}), which conform to the cubic *Fd3(-)m* space group symmetry with hydration–dependent unit cell parameters $a \approx$ 11.80–12.74 nm (Figure 3A and Table S2). This cubic symmetry is consistent with the optically non-birefringent character of these LLC samples. The occurrence of many sharp, high index reflections (*e.g*., (911)) again signifies ordered grain sizes > 100 nm, in these materials especially after thermal cycling to 100 °C. The SAXS pattern and structural symmetry of this sample are wholly consistent with well-known inverse LLC C15 Laves phases, except that the **TMADec-40** LLC is a normal micellar phase.[30, 31, 40] The

reconstructed electron density map for this morphology at w_0 = 12 (Figure 3B) exhibits excellent figures of merit (see Supporting Information for methodological details). This density map reveals 8 large, nearly spherical micelles situated on a diamond lattice, wherein the tetrahedral interstitial sites are filled with tetrahedral groupings of much smaller and slightly deformed micelles (Figure 3C). This spatial particle arrangement is directly analogous to that of the C15 Laves $MgCu_2$ intermetallic compound.[17] Quantitative analyses of this structure demonstrate that these micelles exhibit radii of ~2.02 and ~1.80 nm for the *8a* and *16d* lattice sites, indicating a ~42% volume difference between the different oil-swollen micelles and thus systematic composition differences between each class of symmetry-equivalent particles. We estimate that ~35% of the volume of each micelle core is filled by *n*–decane and that the number of surfactants per *8a* and *16d* micelles is N = 101 and 80, respectively (see Supporting Information for detailed calculations). Neglecting the hydrated counterion cloud, we estimate that the micellar particles comprise an oily core surrounded by a surfactant shell that is ~0.53–0.59 nm thick for this C15 LLC. Closer inspection of this electron density map also shows that the micelles exhibit soft facets, which again mirror the Wigner-Seitz cell structure of the underlying lattice. These oil-filled particles occupy only ~30–35% of the W–S cell volume for their respective lattice sites, with the balance comprising $(CH_3)_4N^+$ counterions and H_2O. While the observed structure is entirely consistent with well-known inverse micellar *Fd3(-)m* phases,[28, 31] these **TMADec-40** LLCs are normal micellar phases with exceptional stability over the temperature range 22 ≤ T ≤ 100 °C. To the best of our knowledge, this normal C15 Laves LLC constitutes the second report of such a structure[51] and the physical mechanism by which it forms has not been elucidated.

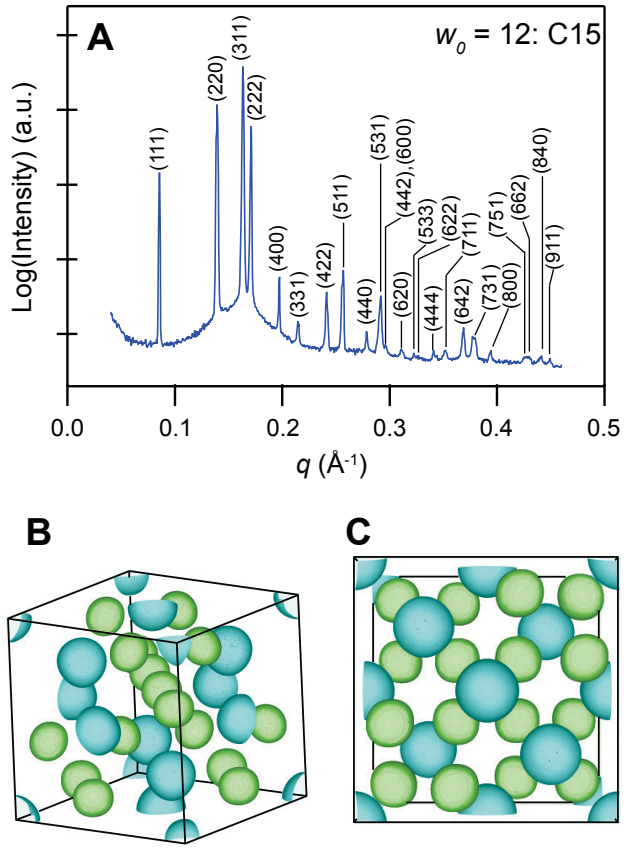

Figure 3. (A) Azimuthally–integrated SAXS powder pattern for the aqueous C15 Laves LLC phase of **TMADec–40** at w_0 = 12 acquired at 25 °C with a cubic unit cell parameter a = 12.74 nm, which exhibits at least 20 distinct peaks, indicative of a high degree of long-range translational order. (B) A view of the electron density map for this C15 phase (90% isosurface) displaying two classes of symmetry-equivalent micelles located in the *8a* (*aqua*) and *16d* (*green*) Wyckoff positions. (C) View of the C15 unit cell electron density map along the (100) direction.

Situated in between the pure C14 and C15 LLC phases, the **TMADec-40** LLC with w_0 = 22 exhibits coexisting C14 and C15 phases (Figure 1). The position of the (002) reflection of the C14 phase notably coincides with that of the (111) reflection of the C15 structure, in a manner

directly analogous to intermetallic compounds,[52] in which these two phases are thermodynamically close in energy and often coexist. Since the layer stacking in the C14 structure may be described as a repeating AABB… motif and that of the C15 phase is AABBCC…,[11] the crystallographic coincidence of the aforementioned reflections is expected. We also note that the surprisingly stiffer texture of the C14 LLC at higher w_0 as compared to that of the C15 phase probably arises from the lower space group symmetry of the former phase, which implies fewer slip systems that permit facile deformation.[11, 53]

At the lowest hydrations w_0 = 2–8, we observed two additional **TMADec-40** LLC phases. Optically birefringent samples with $4 \leq w_0 \leq 8$ exhibit simple SAXS patterns that correspond to hexagonally-packed cylindrical micelles (H_I) with peaks located at $q/q^* = \sqrt{1}, \sqrt{3}, \sqrt{4}$, and $\sqrt{7}$ (q^* = 0.1823 Å^{-1}), with an intercylinder distance of ~4.0 nm (Figure 1). At a composition with w_0 = 10 between that of the pure H and C15 phases, we observe a region in which these two phases coexist. At the lowest hydration w_0 = 2, we obtained azimuthally-integrated SAXS patterns with relative peak positions $q/q^* = \sqrt{2}, \sqrt{3}, \sqrt{4}, \sqrt{5}, \sqrt{8}$, and $\sqrt{9}$ (q^* = 0.1120 Å^{-1}) that correspond to a normal bicontinuous double diamond (D) LLC phase with cubic *Pn3(-)m* symmetry and cell parameter $a \approx$ 5.56 nm (Figure 4A).[54] The lack of optical birefringence in this sample concurs with the cubic space group symmetry deduced from SAXS. While this SAXS intensity profile is nearly identical to that reported for well-known inverse double diamond (D) phases,[54] this **TMADec-40** LLC appears to be the first unambiguously identified normal (Type I) double diamond structure. While its formation is not physically forbidden, Chen and Jin have suggested that normal D phases are less stable than the normal bicontinuous double gyroid structure.[55] We used Le Bail refinement to extract the structure factor amplitudes from this SAXS pattern, which were used as inputs for the *SUPRFLIP* charge–flipping algorithm to reconstruct an electron

density map for this LLC (see Supporting Information for methodological details). This iterative charge flipping method makes no presumptions regarding the sample composition, space group symmetry, nor the phases associated with each reflection. The final electron map predicts the observed SAXS data with high fidelity (residual factor R = 1) and the resulting map exhibits the expected cubic *Pn3(-)m* symmetry. Thus, the electron density map for this normal D phase (Figure 4B) confirms the bicontinuous nature of this network of four-fold lipidic connectors in an aqueous matrix, which resembles the connectivity of known inverse D phases observed in LLCs of monoolein and related lipids.[56]

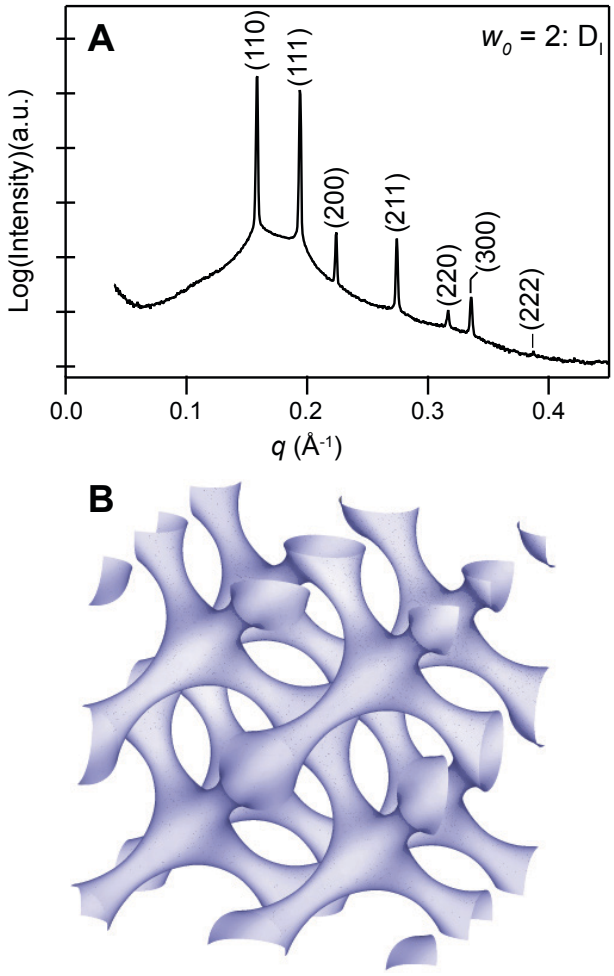

Figure 4. (A) SAXS intensity profile for the

normal double diamond (D_I) morphology formed by hydration of **TMADec–40** with w_0 = 2 at 25 °C, which exhibits a cubic lattice parameter a = 5.56 nm. (B) Electron density map for this D_I phase (90% isosurface), which depicts two interpenetrating networks for four-fold connectors in an aqueous matrix.

The phase behavior of hydrated **TMADec-40** mixtures is graphically depicted in the aqueous LLC phase diagram given in Figure 5. As the water content decreases, we observe the phase sequence BCC → C14 → C15 → H → D. Gibbs' Phase Rule anticipates regions of two-phase LLC coexistence in this phase portrait between each pair of the pure phase windows. However, we only observe H_I/C15 and C14/C15 coexistence windows, likely due to the resolution of our phase map: analyzed samples are separated by headgroup hydration increments Δw_0 = 2 and temperature increments ΔT = 20 °C. While the BCC micellar packing comprises uniform spherical particles packed on a high symmetry lattice as expected for simple surfactant/oil/water mixtures, dehydration of this phase leads to the tetrahedrally closest-packed C14 and C15 Laves phases. The latter structures exhibit multiple classes of symmetry-equivalent, deformed micelles with specific volumes that reflect differences in their oil/surfactant molecular compositions. The symmetry lowering transition from the BCC structure to a series of exceptionally well-ordered FK phases suggests that these phenomena originate from a subtle balance of non-covalent interactions between the micelles. Rappolt and co-workers have previously rationalized the formation of inverse micellar C15 LLC phases, in which the water nanopools are encapsulated by lipids to yield hairy particles, as maximizing the spherical nature of the reverse micelles while minimizing 3D packing frustration of the lipid tails.[32] Bates and co-workers similarly reasoned that the C14, C15, and FK σ phases in compositionally asymmetric diblock polymers arise from maximizing the spherical character of block polymer micelles while packing their corona chains

at constant density.[40-42] However, these arguments do not directly apply to normal LLCs due to the lack of van der Waals contacts between the quasispherical particles.

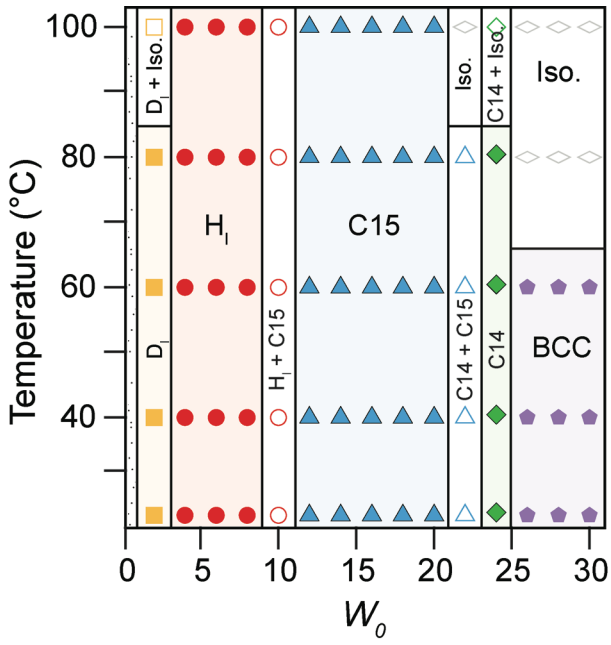

Figure 5. Temperature *versus* surfactant hydration number (w_0) aqueous LLC phase diagram for **TMADec-40**, indicating the composition windows of stability for the normal BCC, C14, C15, H_I, and D_I phases.

Pairwise interactions between the negatively charged, decane-swollen alkylcarboxylate micelles are mediated by the solvated $(CH_3)_4N^+$ counterions situated in the aqueous domains of these spherical LLCs, by analogy to a recent report by Kim *et al.*[33] In order to maximize the electrostatic cohesion in this particle ensemble, the soft and hydrophobic counterions concentrate along midplanes that bisect the directions connecting the centers of neighboring micelles. Thus, the counterions outline the polyhedral boundaries of the *CN* = 12, 15, and 16 Wigner-Seitz cells of the tetrahedrally closest-packed C14 and C15 structures, as well as the truncated octahedral (14-faced) BCC Voronoi cells. Detailed analyses of the electron density map for the C14 phase

provide experimental evidence for this counterion arrangement. Figure 6 depicts a plot of the two-dimensional electron density map (90% isosurface) for the z = ¼ plane (normal to the (002) direction) that cuts through the *6h* micelles shown in Figure 2B. Close inspection of the lower right corner of this map reveals: (1) regions of highest electron density at the oxygen-rich peripheries of the facetted *6h* micelles, and (2) regions of relatively lower electron density at the center of the channels between these micelles (highlighted by dashed *yellow* ovals in Figure 6), which correspond to counterion concentration along the Wigner-Seitz cell boundaries between these *CN* = 12 particles. Since the average locations of the $(CH_3)_4N^+$ counterions are highly correlated with those of the alkylcarboxylate surfactant headgroups,[57] faceting of the counterion clouds drives soft faceting of the micelle cores to minimize variations in the counterion-headgroup distances.

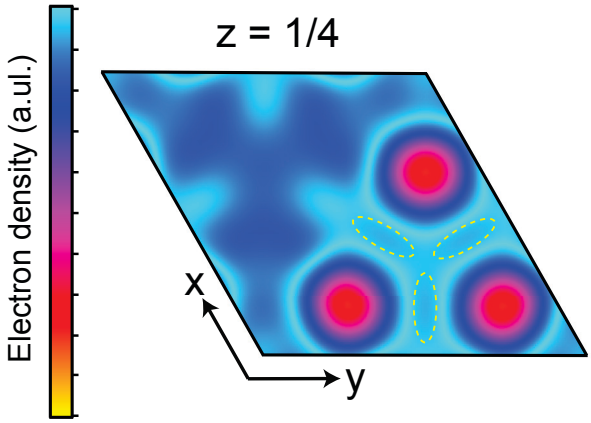

Figure 6. Two-dimensional electron density profile in the z = ¼ plane (90% isosurface) of the C14 Laves LLC phase, in which the lightest blue regions of highest electron density are the carboxylate-rich surfaces of the *6h* micelles. The regions of relatively lower electron density at the centers of the channels between *6h* micelles (outlined in *yellow*) correspond to localized and hydrated $(CH_3)_4N^+$ counterions.

However, isolated micelles in the presence or absence of hydrocarbon oils exhibit a strong thermodynamic preference to form spherically symmetric structures on multiple grounds. A spherical structure minimizes the surface area to volume ratio, thus obviating unfavorable contacts between water and the hydrophobic micelle cores. The uniform curvature of a spherical particle also ensures uniform surfactant headgroup and counterion solvation, consistent with minimizing their solvation free energies. Kim *et al*. coined the term "ionic sphericity" in reference to this particle symmetry preference.[33]

We rationalize the observed sequence of spherical phases BCC → C14 → C15 in terms of maximization of interparticle cohesion within the LLC with maximal ionic sphericity at each hydration. Consider a dilute dispersion of disordered micelles, wherein an abundance of water screens the interactions between the particles. Concentrating this solution results in symmetry breaking to yield a lyotropic mesophase at the critical water concentration ($w_{0,crit}$), where the counterion clouds of adjacent micelles impinge on one another and induce their electrostatic cohesion. In accord with symmetry arguments by Alexander and McTague regarding minimization of the configurational entropy decrease in liquid-to-solid phase transitions,[58] we experimentally observe the formation of a BCC LLC phase in which all lattice sites are symmetry equivalent. Further dehydration of this BCC phase increases the ionic strength of the aqueous matrix, while drawing the micelles closer together. The distance reduction between adjacent lattice sites distorts the micelle counterion clouds to conform to the truncated octahedral shape of the Wigner-Seitz cells of the BCC lattice (14-sided polyhedra). However, faceting of the counterion cloud opposes ionic sphericity. Thus, reduction in the LLC water content drives a transition to a new structure either by particle reconfiguration through molecular exchange of surfactant and oil or by micelle fusion and fission events.

In order to simultaneously maximize ionic sphericity and electrostatic cohesion in the LLC structure, the surfactant and oil molecules redistribute to form a new phase wherein a greater number of neighboring particles surrounds each micelle. The preference for a higher average coordination number (average $CN \geq 12$) in the newly formed lattice originates from the fact that increasing the number of facets on a convex polyhedron renders it more spherical, so that the new packing arrangement maximizes ionic sphericity of the oil-swollen micelles.[33] However, the drive toward local spherical particle symmetry occurs at the expense of reducing the overall LLC lattice symmetry.[27, 42] Thus, complex spherical micelle packings emerge as a consequence of the frustration between local particle symmetry and global lattice energy.

Several groups have predicted the specific sequence of ordered state symmetries expected to materialize from this frustrated supramolecular force balance, by examining the average isoperimetric quotients of various FK crystal lattices.[27, 40, 42, 59] The isoperimetric quotient of a polyhedron is defined as $IQ = 36\pi V^2/S^3$, where V and S are its respective volume and surface area. A perfect sphere has $IQ = 1$, and a value closer to 1 reflects a polyhedral object that more closely approximates a sphere. The number-average isoperimetric quotients for the Wigner-Seitz cells of FK phases decrease in the order:

$$\sigma\ (0.7623) > \text{A15}\ (0.7618) > \text{C14}\ (0.7613) = \text{C15}\ (0.7613)$$

all of which are greater than $IQ(\text{BCC}) = 0.7534$.[40] The phase sequence recently reported by Kim *et al*. in dianionic alkylphosphonate surfactant LLCs as a function of decreasing w_0 reflects this ordering, as a FK A15 phase forms at a lower w_0 than the σ phase.[33] The increased ionic strength in the water domains with decreasing w_0 screens intermolecular repulsions between surfactants in

a given micelle, which allows the micelles to more easily deform and adopt structures with lower ionic sphericities.

We speculate that the notable absence of higher sphericity σ and A15 phases in **TMADec-40** LLCs arises from two factors: (1) chemical differences in the surfactant headgroups, and (2) the presence of *n*-decane as a micelle swelling agent. Alkylphosphonate surfactants form high curvature spherical micelles with low aggregation numbers, as a consequence of the strong intermolecular repulsions between their dianonic headgroups that enforce ionic sphericity.[33] On the other hand, alkylcarboxylate surfactants form relatively larger micelles that are more deformable due to their monoanionic headgroup functionalities, which incur a lesser electrostatic penalty upon deformation. The presence of *n*-decane in the cores of these alkylcarboxylate micelles probably also reduces particle rigidity. *n*-Decane further allows the formation of a broader distribution of discrete micelles sizes, which are necessary for C14 and C15 phase formation. We found that **TMA-Dec** loaded with as little as 10 wt% decane (**TMADec-10**) also forms aqueous LLC C14 and C15 phases, albeit with lower degrees of long-range translational order and somewhat broader SAXS peaks (see Figure S3 for the LLC phase diagram and representative SAXS patterns). In the absence of any oil, our preliminary SAXS analyses demonstrate that **TMA-Dec** forms only G_I, H_I, A15, and BCC LLCs. Previous MD simulations of alkylphosphonate A15 and σ aqueous LLC phases (in the absence of oil) suggest that their micelle volumes only vary by ±10% from their average values.[33] However, micelle radii estimates from the C14 and C15 electron density maps imply variations in the oil-swollen micelle volumes of ± 20% around their average values. We speculate that decoupled surfactant and hydrocarbon exchange through *n*-decane addition enables the formation of a broader micelle

size distribution. Thus, the lower sphericity C14 phase forms instead of the σ phase anticipated by sequence of number-averaged isoperimetric quotients.

Given that the hydrocarbon oil significantly perturbs the structure and rigidity of the micellar particles, one might alternatively argue that different sphericity metrics govern the phase sequences observed in neat surfactants and oil-loaded microemulsions. Instead of number averaging the isoperimetric quotients of each W–S cell as described above, it is possible that the phase sequence observed in LLC microemulsions is determined by the IQ calculated from the number-average surface area and the number-average volume of the lattice W–S cells. This method of averaging instead anticipates the phase sequence:

$$\text{C14 } (0.7650) = \text{C15 } (0.7650) > \sigma\ (0.7632) > \text{A15 } (0.7618),$$

which is consistent with the observed formation of both C14 and C15 phases in aqueous **TMADec-40** LLCs. By analogy to recent self-consistent mean-field theory calculations for spherical morphologies of diblock polymers,[40] the thermodynamic ground state energies of the C14, C15, σ and A15 phases are likely very similar. Nonetheless, exactly how subtle differences in geometry influence the thermodynamics underlying complex LLC sphere packing phase selection remains an open question.

Conclusion

The water concentration-dependent lyotropic self-assembly of simple, single-tail decanoate surfactant micelles swollen with *n*-decane unexpectedly leads to formation of both C15 and C14 normal micellar LLC phases. While isolated oil-swollen micelles in excess water preferentially

form a spherical core surrounded by a spherically symmetric shell of charge-compensating counterions, cohesive interactions between neighboring micelles in ordered LLC lattices drive deviations from counterion cloud sphericity. In order to simultaneously maximize both interparticle cohesion in the ordered lattice and ionic sphericity, oil and surfactant spontaneously reconfigure into micelles with a discrete distribution of sizes and chemical compositions that enable their low symmetry packings. The frustration between maximizing local ionic sphericity of the particles while minimizing global lattice free energy begets the self-assembly of exceptionally well-ordered yet complex LLC phases comprising ~3 nm diameter micelles with grains sizes ≥ 100 nm. The decoupled reconfigurability of particle mass and charge in these ternary oil/water/surfactant mixtures apparently affords exciting opportunities for tuning the observed distribution of particle sizes and their accessible lattice packing symmetries. Given that FK phases are periodic 3D approximants to quasicrystals, subtle manipulation of the identity and amount of added hydrocarbon oil may enable access to liquid quasicrystalline states from relatively simple chemical building blocks.

Methods

Materials. All reagents were purchased from the Sigma–Aldrich Chemical Company (Milwaukee, WI) and used as received. An aqueous solution of $(CH_3)_4NOH$ was titrated with a standardized 1.000 N HCl(*aq*) solution to yield an aqueous base concentration of 1.007 M.

Molecular analysis. ^{1}H and ^{13}C spectra of surfactant samples dissolved in CD_3OD-d_4 were acquired at 24 °C using a Bruker Avance 400 spectrometer. Carbon, hydrogen, and nitrogen combustion analyses were performed by Atlantic Microlab, Inc. (Norcross, GA, USA).

Synthesis of Tetramethylammonium Decanoate (TMA–Dec). A suspension of decanoic acid (11.34 g, 65.85 mmol) in MeOH (150 mL) was stoichiometrically deprotonated with an aqueous solution of $(CH_3)_4NOH$ (65.42 mL, 1.0065 M in H_2O, 65.85 mmol) in a round-bottom flask equipped with stirbar. This mixture was stirred at 22 °C for an additional 2 h after it became homogeneous to ensure complete reaction, after which the volatile solvents were removed under vacuum. The resulting hygroscopic solid was freeze-dried two times, by suspending the solids in C_6H_6 (50 mL), freezing the suspension in $N_2(l)$, and subliming the frozen solvent at reduced pressure. ^{1}H NMR (400.18 MHz, CD_3OD-d_4, 24 °C): δ (ppm) 3.22 (N-CH_3, s, 24H), 2.18–2.14 (CH_2-COO^-, t, 2H), 1.65–1.58 (CH_2-CH_2, m, 2H), 1.36-1.31 (CH_2, m, 12H), 0.93-0.90 (CH_2-CH_3, t, 3H). ^{13}C NMR (100.62 MHz, CD_3OD, 24 °C): δ (ppm) 181.45 (C=O), 54.47 (N(CH_3)$_4$), 47.60 (CH_2), 38.01 (CH_2), 31.68 (CH_2), 29.52 (CH_2), 29.33 (CH_2), 29.29 (CH_2), 29.07 (CH_2), 26.47 (CH_2), 22.34 (CH_2), 13.06 (CH_3). Anal. calc. for $C_{14}H_{31}NO_2$•0.45H_2O: C, 68.52; H, 12.73; N, 5.71. Found: C, 68.31; H, 12.80; N, 5.48.

Lyotropic Liquid Crystal (LLC) Sample Preparation. Aqueous LLCs were prepared by the following two-step procedure. Precisely massed amounts of solid **TMA-Dec** and *n*-decane (40 wt% relative to the surfactant) were combined in 4 mL vials, which were iteratively centrifuged at 4950 × *g* for 10 min at 25 °C and hand-mixed with a spatula three times to yield **TMADec–40**. Ultra-pure water (Type I, 18MΩ•cm) was massed into to the surfactant/oil mixture, after which the ternary microemulsion mixture was centrifuged and hand-mixed three more times to yield optically homogeneous, gel-like solids. All LLC samples thus prepared were pre-annealed at 50 °C for 15 min and allowed to rest at room temperature for a minimum of 24 h prior to X-ray analyses. Samples not in active use were stored in tightly capped vials to avoid any dehydration. The compositions of all **TMADec–40** LLCs are reported in terms of the surfactant headgroup

hydration number w_0 = (total moles of H_2O present)/(moles **TMA-Dec**), where the total number of moles of H_2O includes both the water associated with the **TMA-Dec** surfactant hydrate and the ultra-pure water added.

Synchrotron Small–angle X–ray Scattering (SAXS). A beam energy of 13.30 keV (λ = 0.9322 Å) and sample-to-detector distance of 2.027 m were used at the Advanced Photon Source (Argonne National Laboratory, Argonne, IL) Sector 12-ID-B synchrotron beam line for all SAXS analyses. LLC samples were sealed in hermetic, alodined aluminum DSC pans (TA Instruments, New Castle, DE) to prevent water loss during analyses, and these pans were thermally equilibrated for at least 5 min at the desired temperatures using a Linkam DSC hot-stage, prior to X-ray exposure. Scattering patterns from LLC samples obtained by sample exposure to high intensity X-rays for ≤ 0.1 s were collected on a Pilatus 2M detector (25.4 cm x 29.0 cm rectangular area with 172 μm x 172 μm pixels). The sample to detector distance was calibrated using a silver behenate standard (d = 58.38 Å). 2D–SAXS patterns were azimuthally integrated to generate one–dimensional intensity $I(q)$ *versus* scattering wavevector q ($Å^{-1}$) patterns using the DataSqueeze software package (http://www.datasqueezesoftware.com).

Detailed descriptions of the extraction of the structure factor intensities by Le Bail refinement of the SAXS data using the *JANA2006*[49] crystallographic computing software package, and subsequent application of the charge flipping algorithms implemented in the *SUPERFLIP*[50] software program are provided in the Supporting Information. *SUPERFLIP* text input files from which the electron density maps (90% isosurfaces) in Figures 2–4 were derived are also furnished in the Supporting Information.

ASSOCIATED CONTENT

Supporting Information

The Supporting Information is available free of charge on the ACS Publications website at DOI: 10.1021/acsnano.xxxxxxx.

SAXS data for the thermoreversible BCC to disordered micelles transition, supplemental SAXS data for the C14 LLC phase, tabulated SAXS peak positions and residuals, description of the electron density map reconstruction methodology and *SUPERFLIP* input files for the double diamond, C15, and C14 phases (w_0 = 2, 12, 24, respectively), and representative SAXS data and phase diagram from **TMADec–10** LLCs. (PDF)

AUTHOR INFORMATION

Author Contributions

This manuscript was written through contributions of all authors, and all authors have given approval to the final version of the manuscript.

Acknowledgment

This work was supported by National Science Foundation grant CHE-1608115 and the University of Minnesota–Twin Cities. Synchrotron SAXS analyses were conducted at Sector 12 of the Advanced Photon Source (APS), a U.S. Department of Energy (DOE) Office of Science User Facility operated for the DOE Office of Science by Argonne National Laboratory under Contract No. DE-AC02-06CH11357. Research reported in this publication was also supported by the Office of the Vice President of Research, College of Science and Engineering, and the

Department of Chemistry at the University of Minnesota. We also thank G. Jackson and A. Jayaraman for assistance with analyses of the electron density maps and for helpful discussions.

References

1. Bates, C. M.; Bates, F. S. 50th Anniversary Perspective: Block Polymers—Pure Potential. *Macromolecules* **2017,** *50*, 3-22.

2. Bates, F. S.; Hillmyer, M. A.; Lodge, T. P.; Bates, C. M.; Delaney, K. T.; Fredrickson, G. H. Multiblock Polymers: Panacea or Pandora's Box? *Science* **2012,** *336*, 434-440.

3. Vertogen, G.; de Jeu, W. H., *Thermotropic Liquid Crystals, Fundamentals*. Springer Science & Business Media: 2012; Vol. 45.

4. Tschierske, C. Development of Structural Complexity by Liquid-Crystal Self-Assembly. *Angew. Chem. Int. Ed.* **2013,** *52*, 8828-8878.

5. Huang, M.; Hsu, C. H.; Wang, J.; Mei, S.; Dong, X.; Li, Y.; Li, M.; Liu, H.; Zhang, W.; Aida, T.; Zhang, W. B.; Yue, K.; Cheng, S. Z. Selective Assemblies of Giant Tetrahedra *via* Precisely Controlled Positional Interactions. *Science* **2015,** *348*, 424-428.

6. Yue, K.; Huang, M.; Marson, R. L.; He, J.; Huang, J.; Zhou, Z.; Wang, J.; Liu, C.; Yan, X.; Wu, K.; Guo, Z.; Liu, H.; Zhang, W.; Ni, P.; Wesdemiotis, C.; Zhang, W.-B.; Glotzer, S. C.; Cheng, S. Z. D. Geometry Induced Sequence of Nanoscale Frank–Kasper and Quasicrystal Mesophases in Giant Surfactants. *Proc. Natl. Acad. Sci. U.S.A.* **2016,** *113*, 14195-14200.

7. Neto, A. M. F.; Salinas, S. R., *The Physics of Lyotropic Liquid Crystals: Phase Transitions and Structural Properties*. Oxford University Press: Oxford, 2005; Vol. 62.

8. Kato, T.; Mizoshita, N.; Kishimoto, K. Functional Liquid-Crystalline Assemblies: Self-Organized Soft Materials. *Angew. Chem. Int. Ed.* **2005,** *45*, 38-68.

9. Boyle, B. M.; French, T. A.; Pearson, R. M.; McCarthy, B. G.; Miyake, G. M. Structural Color for Additive Manufacturing: 3D-Printed Photonic Crystals from Block Copolymers. *ACS Nano* **2017,** *11*, 3052-3058.

10. Hustad, P. D.; Marchand, G. R.; Garcia-Meitin, E. I.; Roberts, P. L.; Weinhold, J. D. Photonic Polyethylene from Self-Assembled Mesophases of Polydisperse Olefin Block Copolymers. *Macromolecules* **2009,** *42*, 3788-3794.

11. Hynninen, A.-P.; Thijssen, J. H. J.; Vermolen, E. C. M.; Dijkstra, M.; van Blaaderen, A. Self-Assembly Route for Photonic Crystals with a Bandgap in the Visible Region. *Nat. Mater.* **2007,** *6*, 202-205.

12. Kresge, C. T.; Leonowicz, M. E.; Roth, W. J.; Vartuli, J. C.; Beck, J. S. Ordered Mesoporous Molecular Sieves Synthesized by a Liquid-Crystal Template Mechanism. *Nature* **1992,** *359*, 710-712.

13. Davis, M. E. Ordered Porous Materials for Emerging Applications. *Nature* **2002,** *417*, 813-821.

14. Kim, H.; Leal, C. Cuboplexes: Topologically Active Sirna Delivery. *ACS Nano* **2015,** *9*, 10214-10226.

15. Lynch, M. L.; Spicer, P. T., Eds. Bicontinuous Liquid Crystals. *Surfactant Sci. Ser.* **2005,** *127*, 1-512.

16. Aleandri, S.; Bandera, D.; Mezzenga, R.; Landau, E. M. Biotinylated Cubosomes: A Versatile Tool for Active Targeting and Codelivery of Paclitaxel and a Fluorescein-Based Lipid Dye. *Langmuir* **2015,** *31*, 12770-12776.

17. De Graef, M.; McHenry, M. E., *Structure of Materials: An Introduction to Crystallography, Diffraction and Symmetry*. Cambridge University Press: New York, 2012.

18. Soderlind, P.; Eriksson, O.; Johansson, B.; Wills, J. M.; Boring, A. M. A Unified Picture of the Crystal Structures of Metals. *Nature* **1995,** *374*, 524-525.

19. Moseley, P. T.; Seabrook, C. J. The Crystal Structure of β-Tantalum. *Acta Crystallogr. B* **1973,** *29*, 1170-1171.

20. Hecker, S. S. Plutonium and Its Alloys. *Los Alamos Sci.* **2000,** *26*, 290.

21. Frank, F. C.; Kasper, J. S. Complex Alloy Structures Regarded as Sphere Packings. I. Definitions and Basic Principles. *Acta Crystallogr.* **1958,** *11*, 184-190.

22. Frank, F. C.; Kasper, J. S. Complex Alloy Structures Regarded as Sphere Packings. II. Analysis and Classification of Representative Structures. *Acta Crystallogr.* **1959,** *12*, 483-499.

23. Janot, C., *Quasicrystals—a Primer*. Oxford University Press: Oxford, 1994.

24. Jaric, M. V., *Introduction to Quasicrystals*. 1st ed.; Academic Press: San Diego, 1988; Vol. 1.

25. Ashcroft, N. W.; Mermin, N. D., *Solid State Physics*. Holt, Rinehart, and Winston: New York, 1976.

26. Ungar, G.; Zeng, X. Frank-Kasper, Quasicrystalline and Related Phases in Liquid Crystals. *Soft Matter* **2005,** *1*, 95-106.

27. Grason, G. M. The Packing of Soft Materials: Molecular Asymmetry, Geometric Frustration and Optimal Lattices in Block Copolymer Melts. *Phys. Rep.* **2006,** *433*, 1-64.

28. Shearman, G. C.; Tyler, A. I. I.; Brooks, N. J.; Templer, R. H.; Ces, O.; Law, R. V.; Seddon, J. M. Ordered Micellar and Inverse Micellar Lyotropic Phases. *Liq. Cryst.* **2010,** *37*, 679-694.

29. Vargas, R.; Mariani, P.; Gulik, A.; Luzzati, V. Cubic Phases of Lipid-Containing Systems. *J. Mol. Biol.* **1992,** *225*, 137-145.

30. Luzzati, V.; Vargas, R.; Gulik, A.; Mariani, P.; Seddon, J. M.; Rivas, E. Lipid Polymorphism: A Correction. The Structure of the Cubic Phase of Extinction Symbol *Fd*-- Consists of Two Types of Disjointed Reverse Micelles Embedded in a Three-Dimensional Hydrocarbon Matrix. *Biochemistry* **1992,** *31*, 279-285.

31. Seddon, J. M.; Zeb, N.; Templer, R. H.; McElhaney, R. N.; Mannock, D. A. An Fd3m Lyotropic Cubic Phase in a Binary Glycolipid/Water System. *Langmuir* **1996,** *12*, 5250-5253.

32. Rappolt, M.; Cacho-Nerin, F.; Morello, C.; Yaghmur, A. How the Chain Configuration Governs the Packing of Inverted Micelles in the Cubic Fd3m-Phase. *Soft Matter* **2013,** *9*, 6291-6300.

33. Kim, S. A.; Jeong, K.-J.; Yethiraj, A.; Mahanthappa, M. K. Low-Symmetry Sphere Packings of Simple Surfactant Micelles Induced by Ionic Sphericity. *Proc. Natl. Acad. Sci. U.S.A.* **2017,** *114*, 4072-4077.

34. Percec, V.; Peterca, M.; Tsuda, Y.; Rosen, B. M.; Uchida, S.; Imam, M. R.; Ungar, G.; Heiney, P. A. Elucidating the Structure of the Pm3(-)n Cubic Phase of Supramolecular Dendrimers through the Modification of Their Aliphatic to Aromatic Volume Ratio. *Chem. Eur. J.* **2009,** *15*, 8994-9004.

35. Ungar, G.; Liu, Y.; Zeng, X.; Percec, V.; Cho, W. D. Giant Supramolecular Liquid Crystal Lattice. *Science* **2003,** *299*, 1208-1211.

36. Zeng, X.; Ungar, G.; Liu, Y.; Percec, V.; Dulcey, A. E.; Hobbs, J. K. Supramolecular Dendritic Liquid Quasicrystals. *Nature* **2004,** *428*, 157-160.

37. Chanpuriya, S.; Kim, K.; Zhang, J.; Lee, S.; Arora, A.; Dorfman, K. D.; Delaney, K. T.; Fredrickson, G. H.; Bates, F. S. Cornucopia of Nanoscale Ordered Phases in Sphere-Forming Tetrablock Terpolymers. *ACS Nano* **2016,** *10*, 4961-4972.

38. Gillard, T. M.; Lee, S.; Bates, F. S. Dodecagonal Quasicrystalline Order in a Diblock Copolymer Melt. *Proc. Natl. Acad. Sci. U.S.A.* **2016,** *113*, 5167-5172.

39. Lee, S.; Bluemle, M. J.; Bates, F. S. Discovery of a Frank-Kasper σ Phase in Sphere-Forming Block Copolymer Melts. *Science* **2010,** *330*, 349-353.

40. Kim, K.; Schulze, M. W.; Arora, A.; Lewis, R. M.; Hillmyer, M. A.; Dorfman, K. D.; Bates, F. S. Thermal Processing of Diblock Copolymer Melts Mimics Metallurgy. *Science* **2017,** *356*, 520.

41. Schulze, M. W.; Lewis, III, R. M.; Lettow, J. H.; Hickey, R. J.; Gillard, T. M.; Hillmyer, M. A.; Bates, F. S. Conformational Asymmetry and Quasicrystal Approximants in Linear Diblock Copolymers. *Phys. Rev. Lett.* **2017,** *118*, 207801.

42. Lee, S.; Leighton, C.; Bates, F. S. Sphericity and Symmetry Breaking in the Formation of Frank-Kasper Phases from One Component Materials. *Proc. Natl. Acad. Sci. U.S.A.* **2014,** *111*, 17723-17731.

43. Zeng, X.; Liu, Y.; Impéror-Clerc, M. Hexagonal Close Packing of Nonionic Surfactant Micelles in Water. *J. Phys. Chem. B* **2007,** *111*, 5174-5179.

44. Shearman, G. C.; Tyler, A. I. I.; Brooks, N. J.; Templer, R. H.; Ces, O.; Law, R. V.; Seddon, J. M. A 3-D Hexagonal Inverse Micellar Lyotropic Phase. *J. Am. Chem. Soc.* **2009,** *131*, 1678-1679.

45. Liu, C. K.; Warr, G. G. Hexagonal Closest-Packed Spheres Liquid Crystalline Phases Stabilised by Strongly Hydrated Counterions. *Soft Matter* **2014,** *10*, 83-87.

46. Stewart, J. A.; Saiani, A.; Bayly, A.; Tiddy, G. J. T. Phase Behavior of Lyotropic Liquid Crystals in Linear Alkylbenzene Sulphonate (LAS) Systems in the Presence of Dilute and Concentrated Electrolyte. *J. Dispersion Sci. Technol.* **2011,** *32*, 1700-1710.

47. Perroni, D. V.; Baez-Cotto, C. M.; Sorenson, G. P.; Mahanthappa, M. K. Linker Length-Dependent Control of Gemini Surfactant Aqueous Lyotropic Gyroid Phase Stability. *J. Phys. Chem. Lett.* **2015,** *6*, 993-998.

48. Hajiw, S.; Pansu, B.; Sadoc, J.-F. Evidence for a C14 Frank–Kasper Phase in One-Size Gold Nanoparticle Superlattices. *ACS Nano* **2015,** *9*, 8116-8121.

49. Petříček, V.; Dušek, M.; Palatinus, L. Crystallographic Computing System *JANA2006*: General Features. *Z. Kristallogr. Cryst. Mater.* **2014,** *229*, 345–352.

50. Palatinus, L.; Chapuis, G. *SUPERFLIP*–A Computer Program for the Solution of Crystal Structures by Charge Flipping in Arbitrary Dimensions. *J. Appl. Crystallogr.* **2007,** *40*, 786-790.

51. de Geyer, A.; Guillermo, A.; Rodriguez, V.; Molle, B. Evidence for Spontaneous Formation of Three-Dimensionally Periodic Cellular Structures in a Water/Oil/Surfactant/Alcohol System. *J. Phys. Chem. B* **2000,** *104*, 6610-6617.

52. Stein, F.; Palm, M.; Sauthoff, G. Structure and Stability of Laves Phases. Part I. Critical Assessment of Factors Controlling Laves Phase Stability. *Intermetallics* **2004,** *12*, 713-720.

53. Callister, W. D.; Rethwisch, D. G., *Materials Science and Engineering*. John Wiley & Sons: New York, 2011; Vol. 5.

54. Hyde, S. T., Chapter 16: Identification of Lyotropic Liquid Crystalline Mesophases in *Handbook of Applied Surface and Colloid Chemistry*, Holmberg, K., Ed. John Wiley & Sons, Ltd.: New York, 2001; Vol. 2, pp 299-332.

55. Chen, H.; Jin, C. Competition Brings out the Best: Modelling the Frustration between Curvature Energy and Chain Stretching Energy of Lyotropic Liquid Crystals in Bicontinuous Cubic Phases. *Interface Focus* **2017,** *7*.

56. Kulkarni, C. V.; Wachter, W.; Iglesias-Salto, G.; Engelskirchen, S.; Ahualli, S. Monoolein: A Magic Lipid? *Phys. Chem. Chem. Phys.* **2011,** *13*, 3004-3021.

57. Mantha, S.; McDaniel, J. G.; Perroni, D. V.; Mahanthappa, M. K.; Yethiraj, A. Electrostatic Interactions Govern “Odd/Even” Effects in Water-Induced Gemini Surfactant Self-Assembly. *J. Phys. Chem. B* **2017,** *121*, 565-576.

58. Alexander, S.; McTague, J. Should All Crystals Be BCC? Landau Theory of Solidification and Crystal Nucleation. *Phys. Rev. Lett.* **1978,** *41*, 702-705.

59. Rivier, N. Kelvin's Conjecture on Minimal Froths and the Counter-Example of Weaire and Phelan. *Philos. Mag. Lett.* **1994,** *69*, 297-303.